Effects of heat treatment on the structure and magnetic properties of Al-Ge added $Fe_{73.5-x}Si_{13.5}B_9Nb_3Cu$ alloys

F. Shahri,[1] A. Beitollahi,[1,*] S. G. Shabestari,[1] and S. Kamali[2]

[1]*Nanomaterial Group, Department of Metallurgy and Materials Engineering, Iran University of Science and Technology (IUST), Narmak, Farjam, Tehran, Iran*

[2]*Department of Physics, the Angstrom Laboratory, Uppsala University, Box 530, SE-751 21 Uppsala, Sweden*

(Received 3 February 2007; revised manuscript received 30 April 2007; published 27 July 2007)

In this work, we have studied the effects of the coaddition of Al(1.5 at. %)/Ge(1 at. %) and heat-treatment temperature on the structure and magnetic properties of rapidly quenched pure $Fe_{73.5-x}Si_{13.5}B_9Nb_3Cu$ (FINEMET) alloys prepared by the single roller melt spinning process. Two series of as-spun and heat-treated alloys, 400, 480, 560, 640, and 730 °C for 1 h in vacuum (10^{-6} Torr), were studied using various techniques such as x-ray diffraction (XRD), transmission electron microscopy (TEM), differential scanning calorimetry (DSC), Mössbauer spectroscopy, and *B-H* loop tracer. Mössbauer analysis carried out on both series of alloys heat treated at 560 °C revealed the presence of two phases, Fe_3Si phase with $D0_3$ structure and a residual amorphous phase with reduced hyperfine field (16.9 T) compared to those of Al/Ge added (22.5 T) and pure FINEMET (~23.4 T) alloys, in close agreement with XRD and TEM results. The highest maximum permeability, saturation magnetization, and the lowest coercivity were obtained for both series of alloys when heat treated at 560 °C. However, the magnitude of coercivity was lower for the Al/Ge substituted alloy (heat treated at 560 °C) compared to that of the pure FINEMET alloy. This is due to the substitution of Al atoms for Fe as confirmed by our XRD and Mössbauer results. Further, a higher ferromagnetic amorphous phase Curie temperature ($T_{C,am}$) was detected for the Al/Ge added alloy (322 °C) compared to that of the pure FINEMET alloy (317 °C), which is believed to be mainly related to the presence of Ge atoms in the amorphous matrix. Furthermore, the removal of stress and the setup of nanocrystallization for both series of alloys gave rise to a higher collinear magnetic moment angle. However, this was not the case for the samples heat treated at temperatures above 560 °C, for which the formation of the Fe-B hard magnetic phase was confirmed by our XRD, TEM, and Mössbauer results. Finally, the structural-magnetic properties relationship is discussed for various samples studied in this work.

DOI: 10.1103/PhysRevB.76.024434 PACS number(s): 75.50.Kj, 75.50.Bb, 75.75.+a

I. INTRODUCTION

Fe-based metallic glass ribbons in the Fe-Si-B-Nb-Cu alloy system, known as FINEMET, have attracted wide interest because of their remarkably soft magnetic properties.[1–3] This alloy in amorphous state is produced by a rapid quenching method using the melt spinning technique in ribbon form. the nanocrystallization process applied through controlled crystallization of amorphous ribbons for these alloys gives rise to interesting properties that are otherwise absent in amorphous or microcrystalline forms.[4,5] It is shown that the appropriate heat treatment of this family of alloys of nominal composition $Fe_{73.5}Cu_1Nb_3Si_{13.5}B_9$ produces a homogeneous ultrafine grain structure of α-FeSi with a typical grain diameter of 10 nm embedded in an amorphous matrix.[6] This causes a drastic reduction in the magnitudes of saturation magnetostriction (λ_S) and the intrinsic coercivity ($_iH_C$) due to the formation of well coupled Fe nanocrystallites by exchange interaction, thus favoring easy magnetization and simultaneously higher permeabilities.

The improvement of the soft magnetic properties of various metallic alloys mainly relies on the proper selection and design of the main alloy composition and/or additives and development of the appropriate microstructure and phase(s) through suitable heat-treatment conditions. For the FINEMET alloys, such a trend has also been followed by studying the effects of both the substitution of various elements[7–11] and heat-treatment conditions.[9,12,13] Among the various additives studied, the substitution of small amounts of Al for Fe atoms has been reported[9] to decrease the magnetocrystalline anisotropy and hence intrinsic coercivity ($_iH_C$). On the other hand, the addition of Ge in FINEMET alloys has also been reported[14] to increase the Curie temperature of the amorphous matrix phase ($T_{C,am}$). At temperatures near $T_{C,am}$, i.e., near the ferromagnetic-paramagnetic transition of the amorphous phase, magnetic hardening appears due to magnetic decoupling of Fe-Si grains, limiting the application temperature of these alloys. The work presented here was therefore stimulated by considering the possible advantages of coaddition of both of the above mentioned additives. Here, we report the effects of coaddition of Al(1.5 at. %)/Ge(1 at. %) and heat-treatment temperature on the microstructure and/or structure and magnetic properties of FINEMET alloys. In this respect, phase evolutions taking place at various heat-treatment temperatures were investigated using Mössbauer spectroscopy as a powerful tool to study structural variations, site occupancy, and magnetic structure and/or moment orientations, accomplishing other characterization techniques used in this work, such as x-ray diffraction (XRD), transmission electron microscopy (TEM), differential scanning calorimetry (DSC), and magnetic measurements.

II. EXPERIMENT

Amorphous Fe-based ribbons, of nominal compositions $Fe_{73.5}Si_{13.5}B_9Nb_3Cu_1$ (hereafter referred to as Al_0Ge_0 alloy)

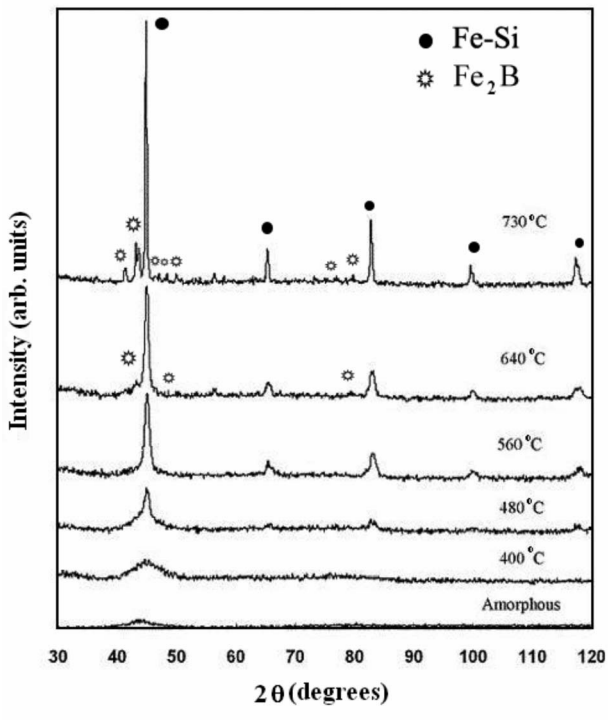

FIG. 1. XRD patterns of the as-spun and heat-treated Al_0Ge_0 alloys.

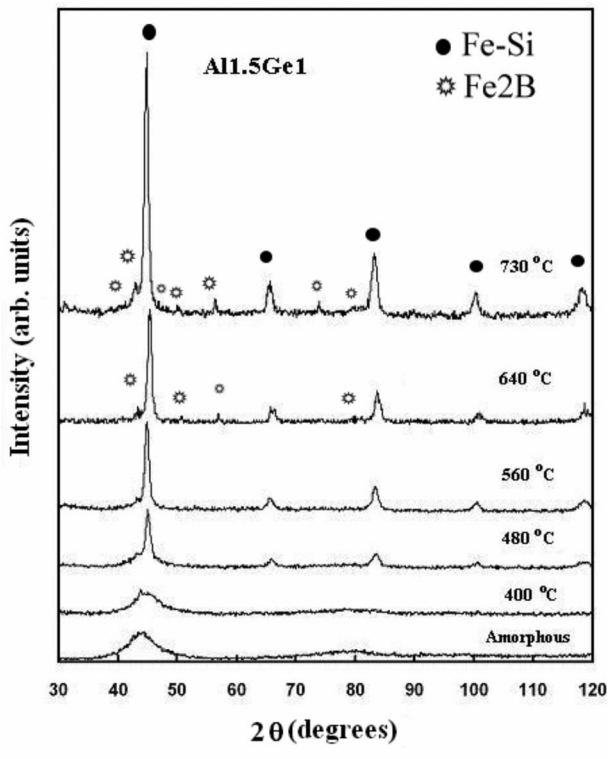

FIG. 2. XRD patterns of the as-spun and heat-treated $Al_{1.5}Ge_1$ alloys.

and $Fe_{71}Si_{13.5}B_9Nb_3Cu_1Al_{1.5}Ge_1$ (hereafter referred to as $Al_{1.5}Ge_1$ alloy) were prepared by the single roller melt spinning process at a wheel speed of 25 m/s using extrapure constituting elements. The as-spun samples were heat treated at various temperatures, 400, 480, 560, 640, and 730 °C, for 1 h in a vacuum furnace. The crystalline structures of the as-spun and heat-treated samples were examined by the XRD technique using Cu $K\alpha_1$ radiation. The lattice parameters were calculated using the Nelson-Riley extrapolation method.[15] The average crystallite sizes of the samples were also determined from the full width at half maximum of the strongest reflection, the (220) peak, using the Williamson-Hall method[16] after applying the standard correction for instrumental broadening. The microstructural study of the as-spun and heat-treated samples was carried out using a 200 kV Philips TEM. The crystallization kinetics of the as-spun samples were examined with a DSC under ultrapure argon (99.9999%) atmosphere at a 20 K/min heating rate. The static *B-H* loops of the samples were determined using a *B-H* loop tracer on ring shaped wire wound ribbons. The room temperature maximum relative permeability of the samples at 10 kHz was also measured using an automatic *LCR* meter on ring shaped samples. Further, for room temperature ^{57}Fe Mössbauer spectroscopic measurements, ^{57}Co in a Rh matrix was used at room temperature as the source. The spectra were calibrated by using the six lines of α-Fe, the center of which was taken as zero isomer shift (IS). The Mössbauer spectra were fitted using the RECOIL program[17] with the Voigt-based method, where the magnetic hyperfine parameter distributions are represented by a sum of Gaussian components. The samples were put together on a tape to form thin foils and the direction of the incoming photons was perpendicular to the plane of the foils.

III. RESULTS AND DISCUSSION

A. Structural and/or microstructural analysis

Figures 1 and 2 show XRD patterns of the as-spun and heat-treated Al_0Ge_0 and $Al_{1.5}Ge_1$ samples, respectively. As can be realized from these patterns, for as-spun samples, only one broad peak around $2\theta=45°$ could be noticed, indicating that these samples were amorphous.

This was also confirmed by our TEM results. Figure 3 demonstrates a typical TEM micrograph and the corresponding single area diffraction pattern (SADP) obtained for the

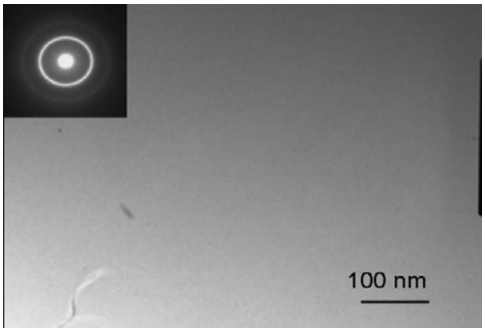

FIG. 3. Typical TEM micrograph as well as SADP for the as-spun Al_0Ge_0 alloys.

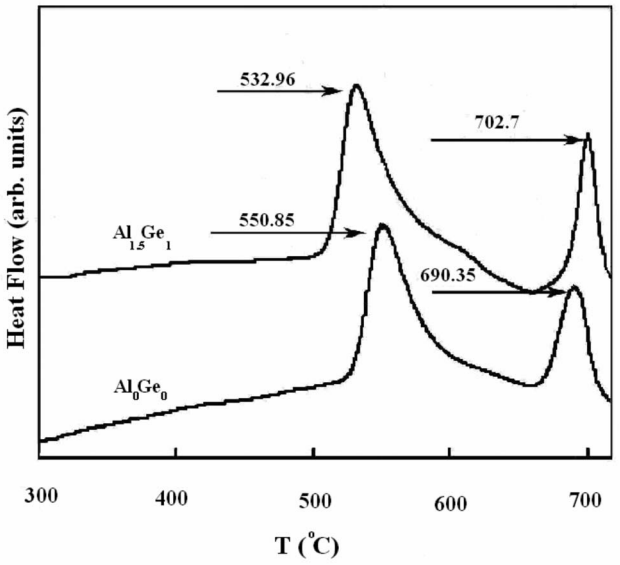

FIG. 4. DSC curves of both series of alloys, (a) Al_0Ge_0 and (b) $Al_{1.5}Ge_1$, obtained at a heating rate of 20 K/min in ultrapure argon gas.

as-spun Al_0Ge_0 alloy. The presence of halo diffraction rings for Al_0Ge_0 alloy (Fig. 3) and as-spun $Al_{1.5}Ge_1$ alloys (not shown here) supported the formation of amorphous structure. Figure 4 also displays the DSC curves of both series of as-spun alloys obtained at a constant heating rate of 20 K/min. As shown in Fig. 4, two sets of strong exothermic peaks were detected for each of these two alloys. For the Al_0Ge_0 alloy, the first one appeared at about 551 °C and was attributed to the primary crystallization of the nanocrystalline phase, i.e., Fe(Si) soft ferromagnetic phase, and the second one appeared at ~691 °C and was related to the formation of iron boride phase(s). The primary and second crystallization peaks for the $Al_{1.5}Ge_1$ alloy, however, appeared at two different temperatures, i.e., ~533 and ~703 °C, respectively.

The comparison of the DSC data obtained for these two series of alloys suggests that the coaddition of Al/Ge, on one hand, shifted the primary crystallization peak toward lower temperatures but, on the other hand, moved the position of the second crystallization peak [corresponding to the boride phase(s)] to higher temperatures compared to those of the Al_0Ge_0 alloy. It is worthy to note that the observed shift of the second crystallization peak related to boride phase(s) toward higher temperatures for $Al_{1.5}Ge_1$ alloy is advantageous since the formation of boride phase(s) is seen to affect adversely the excellent soft magnetic behavior of these alloys.

Based on our XRD results, the amorphous structures observed for the as-spun samples did not change much when annealed at 400 °C (Figs. 1 and 2). However, increasing the heat-treatment temperature to 480 °C revealed the early signs of crystallization steps for both series of alloys, evidenced by the appearance of diffraction peaks in their XRD patterns. Further, the intensities of the crystalline diffraction peaks were higher for the $Al_{1.5}Ge_1$ alloy compared to those of the Al_0Ge_0 alloy when heat treated at 480 °C. Increasing the heat-treatment temperature to 560 °C gave rise to higher

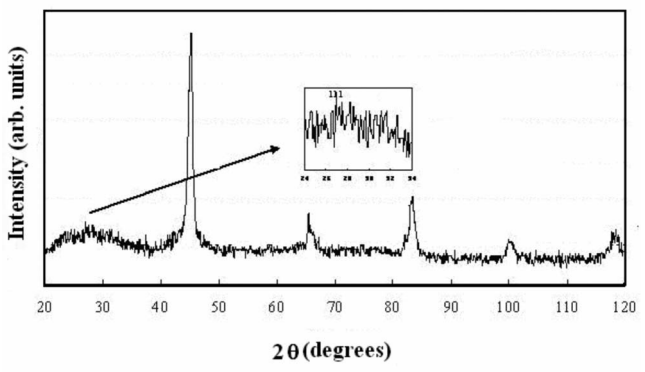

FIG. 5. XRD pattern of the $Al_{1.5}Ge_1$ alloys heat treated at 560 °C. The inset shown in this figure highlights the presence of very weak (111) superlattice reflection.

intensities of the observed diffraction peaks (Figs. 1 and 2). The observed diffraction peaks for both series of alloys heat treated at 560 °C could be indexed as Fe_3Si phase with $D0_3$ structure. The existence of the $D0_3$ structure was justified by observing the superlattice (111) reflections of very weak intensity in the XRD patterns of both series of alloys heat treated at 560 °C. Figure 5 displays the XRD pattern of $Al_{1.5}Ge_1$ alloy heat treated at 560 °C for which the presence of superlattice (111) reflections is shown as an inset for clarity. The formation of the $D0_3$ structure was also later confirmed by our Mössbauer results, which will be discussed later.

For the samples heat treated above 560 °C, however, some other extra phase could be detected along with the main Fe_3Si phase for both series of alloys (Figs. 1 and 2). The observed extra phase that appeared in the XRD patterns of both series of alloys heat treated at 640 and 730 °C could be indexed as Fe_2B phase. The formation of these two phases was in agreement with our DSC results. It is known that up to 10 at. % silicon is soluble in bcc iron, randomly substituting iron atoms. A further increase of the silicon content leads to a phase transition toward the ordered $D0_3$ structure which exists between about 10 and 30 at. % Si.[18] The lattice parameter of the $D0_3$ crystal structure is roughly twice as large as that of the α-Fe phase and the unit cell consisting of 16 atoms. Two cubic sublattices are present: one of these, designated as A, consists of eight iron atoms, whereas the other, D, contains both iron and silicon. In the stoichiometric compound Fe_3Si, the sublattice D is completely ordered, thus containing equal numbers of D_{Fe} and D_{Si} sites. If the silicon content is less than 25 at. %, Fe atoms occupy some of the D_{Si} sites randomly, thus giving additional iron sites.

For the Al_0Ge_0 sample, the Si content in the Fe_3Si phase calculated based on XRD data was about 15 at. % while for the $Al_{1.5}Ge_1$ alloy, the exact determination of Si content in the Fe(Si) phase was not possible by the XRD technique because of the opposing actions of Si and aluminum atoms. Al atoms tend to expand the lattice while Si atoms cause it to contract.[19]

The calculated lattice parameters based on XRD results for the Al_0Ge_0 and $Al_{1.5}Ge_1$ alloys heat treated at 560 °C were 0.5655 and 0.5662 nm, respectively. The observed in-

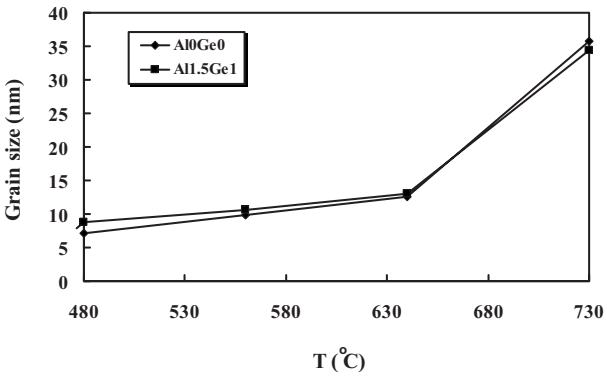

FIG. 6. Variations of average grain sizes of the Fe_3Si phase versus heat-treatment temperatures for both series of alloys.

crease of the lattice parameter in the case of the $Al_{1.5}Ge_1$ alloy is possibly due to the higher atomic radius of Al (143 pm) atoms compared to that of the Fe (124 pm) atoms, since it is believed[9] that Al atoms are substituted for Fe atoms in the Fe_3Si phase. Three dimensional atom probe (3DAP) analysis of 2 at. % Al-containing FINEMET alloys has provided evidence that the Al addition is partitioned to the Fe(Si) crystallites preferentially over the amorphous matrix phase.[20] Further, the atomic radius of Ge (122 pm) is not much different from that of Fe atoms.

For the Al_0Ge_0 and $Al_{1.5}Ge_1$ alloys heat treated at 560 °C, the mean calculated grain sizes of the Fe_3Si grains calculated by Sherrer's formula[15] were ~11.6 and ~12.5 nm, respectively, suggesting that the substitutions of Al(1.5 at.%)/Ge(1 at. %) in pure FINEMET alloy did not give rise to an appreciable change in the average grain sizes of this alloy when heat treated at 560 °C. Figure 6 displays the variations of the calculated average grain sizes of these two series of alloys versus the heat-treatment temperatures.

As can be seen from this figure, mainly two different grain growth rates could be noticed for the samples heat treated between 400 and 730 °C: a slower grain growth rate for the samples heat treated between 480 and 640 °C compared to those heat treated above 640 °C (Fig. 6). It should be mentioned that different diffusion rates can be anticipated for different atomic species which could vary in different ways as the crystallization progresses. Previous studies[21] have reported the presence of high contents of refractory elements such as Nb and B atoms at the periphery of crystalline grains in FINEMET alloys. The Nb-B clusters formed can act as a diffusion barrier and will hence inhibit Fe-Si grain growth. Moreover, it is assumed that the Nb-B segregation is one of the main phenomena responsible for the increase of the local activation energy.[22] For both series of alloys heat treated at 730 °C, the observed sharp rise of the average grain size compared to that of the samples heat treated at 560 °C was in agreement with previous reports[23,24] (Fig. 6).

Figures 7 and 8 also demonstrate the TEM bright field micrograph of Al_0Ge_0 and $Al_{1.5}Ge_1$ samples annealed at 560 °C, respectively.

The formation of crystalline Fe_3Si phase embedded in an amorphous phase could be verified for both series of alloys,

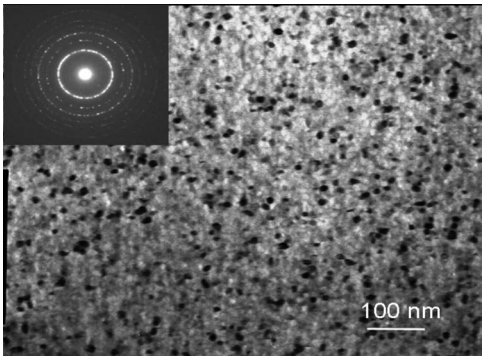

FIG. 7. TEM bright field image and corresponding SADP of Al_0Ge_0 alloy heat treated at 560 °C.

based on their corresponding SADPs obtained (insets shown in Figs. 7 and 8). The average grain sizes of the Fe_3Si phase obtained by TEM for Al_0Ge_0 and $Al_{1.5}Ge_1$ alloys were ~10 and ~12 nm, respectively, i.e., in close agreement with those obtained by Scherrer's formula.[15] Furthermore, TEM examinations carried out for the samples heat treated at 730 °C also confirmed the coexistence of the Fe_2B phase along with the main Fe_3Si phase of $D0_3$ structure, as well as small amounts of residual amorphous phase. Figures 9(a) and 9(b) demonstrate the typical TEM micrographs of the $Al_{1.5}Ge_1$ alloy heat treated at 730 °C with different magnifications. The increased size of the Fe_3Si grains can be readily noticed for this sample compared to those of the samples heat treated at 560 °C (Fig. 8). Further, the TEM–energy dispersive spectroscopy (EDS) analysis carried out for the Fe_2B second phase (Fig. 10) revealed the existence of Nb atoms in this phase with no signs of dissolution of Al or Ge atoms in this extra phase.

B. Mössbauer study

Room temperature Mössbauer spectra of both series of alloys in as-spun and heat-treated states are presented in Figs. 11(a) and 11(b).

Further, Table I also summarizes various refined parameters for these two series of alloys. The Mössbauer spectra obtained for the as-spun samples exhibited broadened Zee-

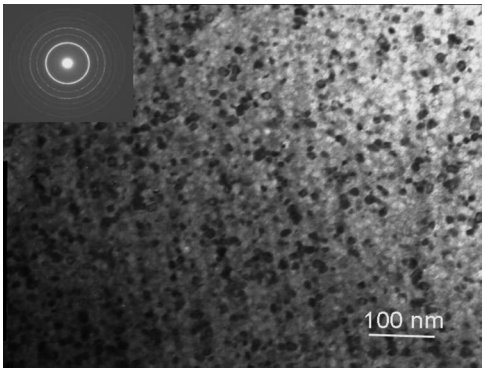

FIG. 8. TEM bright field image and corresponding SADP of $Al_{1.5}Ge_1$ alloy heat treated at 560 °C.

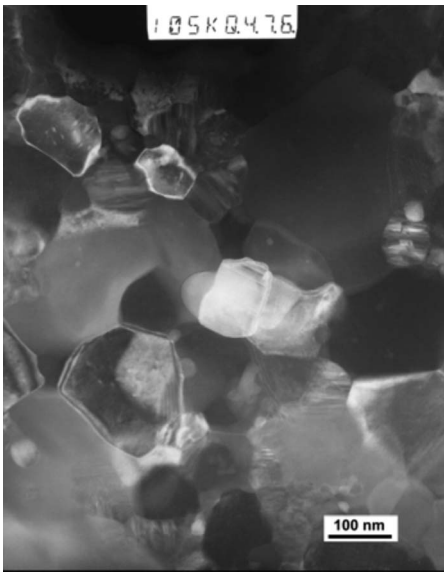

(a)

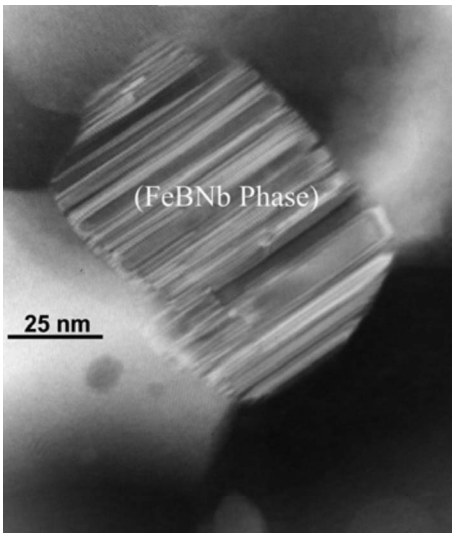

(b)

FIG. 9. TEM micrographs of $Al_{1.5}Ge_1$ alloy heat treated at 730 °C at different magnifications.

man sextets which is typical for fully amorphous FINEMET alloys,[25] in agreement with our XRD and TEM results. For both series of alloys heat treated at 400 °C, a broad sextet [Figs. 11(a) and 11(b)] ascribed to a large distribution of hyperfine fields [Figs. 12(a) and 12(b)] could still be seen, suggesting that no major crystallization has taken place at this temperature for these alloys. It is already reported that heat treatment of as-spun FINEMET alloys at temperatures below the onset of crystallization could mainly give rise to atomic relaxation of the amorphous phase.[26] The hyperfine magnetic field distribution $P(B_{hf})$ curves for both series of alloys in the as-spun state and heat treated at 400 °C show broad bimodal shapes [Figs. 12(a) and 12(b)]. The bimodal

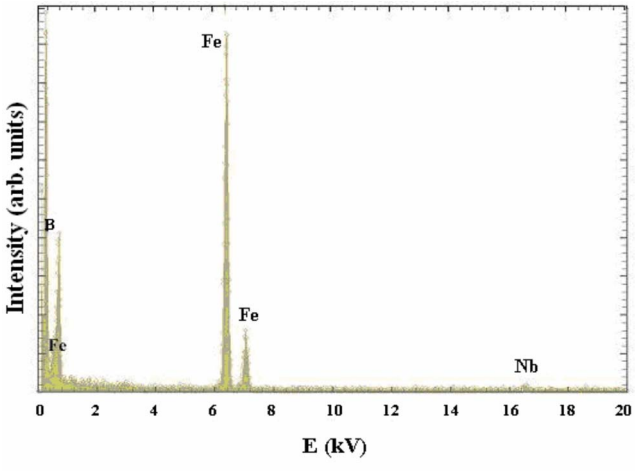

FIG. 10. (Color online) TEM-EDS analysis of the Fe-Nb-B second phase observed for the $Al_{1.5}Ge_1$ alloy heat treated at 730 °C.

behavior can be interpreted as due to the presence of two magnetically distinct types of iron sites.

For the as-spun samples, the $P(B_{hf})$ distributions revealed two major broad peaks: one centered at ~22 T and another at ~12 T. However, these two were shifted slightly toward higher fields for both series of alloys when heat treated at 400 °C. The observed broad peak at low hyperfine fields can be possibly ascribed to Fe atoms preferentially surrounded by Cu, Nb, and B atoms, i.e., attributed to the formation of Cu clusters,[27] while the high one is attributed to those surrounded by Si and B atoms.[28] The low magnitude of B_{hf} is rather close to that of the Cu-Fe solid solutions.[29] Further, the comparison of $P(B_{hf})$ curves for as-spun Al_0G_0 and $Al_{1.5}Ge_1$ alloys also revealed a slight shift in the position of these peaks toward higher fields [Figs. 12(a) and 12(b)]. The slight mentioned shift in the position of $P(B_{hf})$ peaks for the as-spun $Al_{1.5}Ge_1$ alloy compared to that of the as-spun Al_0G_0 alloy is possibly related to local chemistry modifications of the short range ordered clusters due to Al/Ge incorporation in this alloy. Further, the observed shifts of $P(B_{hf})$ peaks for the samples heat treated at 400 °C compared to those of as-spun alloys also highlight the local chemical changes induced by heat treatment of these alloys at this temperature. The hyperfine field depends on the magnetic surroundings, i.e. the chemical surroundings. The Mössbauer spectra obtained for the alloys heat treated above 400 °C indicated the onset of crystallization for both series of alloys. Figure 13 demonstrates the variations of crystallization fraction (in percent) estimated from Mössbauer spectra versus heat-treatment temperatures for both series of alloys studied in this work.

A higher degree of crystallization was obtained for $Al_{1.5}Ge_1$ samples heat treated at 480 and 560 °C, in agreement with our XRD and DSC results. For example, the crystalline fraction of the $Al_{1.5}Ge_1$ alloy annealed at 480 °C was ~39%, while this was only about 31% for the pure FINEMET alloy heat treated at the same temperature. As mentioned before, the DSC results confirmed the setup of a lower crystallization temperature (~533 °C) for $Al_{1.5}Ge_1$ alloys compared to that of Al_0Ge_0 alloy (551 °C). The Möss-

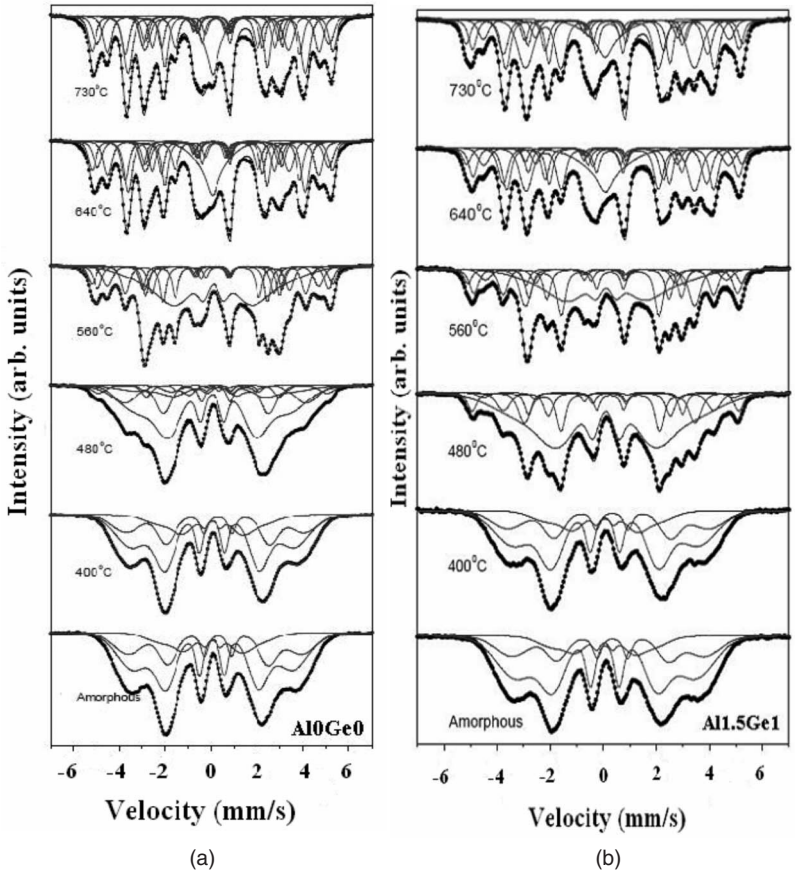

FIG. 11. Mössbauer spectra of the as-spun and heat-treated samples, (a) Al_0Ge_0 and (b) $Al_{1.5}Ge_1$, at various temperatures.

bauer spectra obtained for the as-spun and those heat treated at 400 °C could be fitted by three independent distributed profiles of different hyperfine magnetic fields. These are possibly related to the presence of ultrafine short range ordered Fe clusters with different local chemistries and environments. For all of the samples heat treated above 480 °C, these three components were merged together and the amorphous parts of the samples could be represented just by one component (component A_1 in Table I). Figure 14 also displays the variations of the average hyperfine magnetic field of the amorphous phase $\langle B_{\mathrm{hf,am}}\rangle$ versus heat-treatment temperatures. As can be seen in this figure, while $\langle B_{\mathrm{hf,am}}\rangle$ increased slightly for the amorphous samples when heat treated at 400 °C, this parameter declined sharply for the rest of the heat-treated samples.

The observed initial rise of $\langle B_{\mathrm{hf,am}}\rangle$ highlights the presence of higher Fe concentrations for the samples heat treated at 400 °C. This is possibly related to Cu clustering prior to the onset of the primary crystallization reaction. Hono *et al.*[30] have already shown that Cu atoms form clusters prior to the onset of the primary crystallization reaction. These Cu clusters serve as heterogeneous nucleation sites for the primary crystallization of α-Fe. Further, in FINEMET alloys, silicon concentration in the α-Fe phase in the very early crystallization stage is lower than that in the final microstructure. Based on the 3DAP technique, it is shown[30] that Si atoms do not partition in the α-Fe phase from the very early stage of crystallization and the concentration of Si in the α-Fe appears to be lower than that in the amorphous matrix at the beginning and Si partitioning occurs during the growth stage, and not at the nucleation stage, and hence the α-Fe would have a much lower degree of order than the α-Fe in optimum microstructure. It is suggested[30] that Si is initially depleted from the α-Fe phase, possibly because it is dragged with Nb atoms to the remaining amorphous phase at the beginning. However, by further increase of heat-treatment temperature, the rate of both diffusion of Si into α-Fe and nucleation of Fe-Si phase increases, and hence the amorphous phase will be gradually depleted from Fe atoms, and hence $\langle B_{\mathrm{hf,am}}\rangle$ is expected.

It is interesting to note that the magnitudes of $\langle B_{\mathrm{hf,am}}\rangle$ were lower for all of $Al_{1.5}Ge_1$ alloys compared to those of Al_0Ge_0 alloys (Fig. 14). This could be related to both the lower concentration of Fe atoms used in the initial composition of $Al_{1.5}Ge_1$ alloy and the observed higher crystallization degree for the Fe_3Si phase (Fig. 13).

The onset of nanocrystallization could be realized by the presence of components of narrower magnetic hyperfine distributions. For the $Al_{1.5}Ge_1$ alloy heat treated at 480 °C, the Mössbauer spectra evidenced the onset of primary crystallization. However, the observed intensities of the Mössbauer peaks related to the onset of primary crystallization for Al_0G_0 alloy heat treated at 480 °C was not as strong as those observed for $Al_{1.5}Ge_1$ alloy heat treated at the same temperature [Figs. 11(a) and 11(b)]. This was in close agreement with our XRD and DSC results. Furthermore, rather similar Mössbauer spectra were obtained for both series of alloys when heat treated at 560 °C. All of the nanocrystalline samples have been fitted by superimposing sextets of Lorent-

TABLE I. Summary of various refined Mössbauer parameters: the magnetic hyperfine fields B_{hf}, isomer shift IS, and intensities I of the different components of both series of (a) Al_0Ge_0 and (b) $Al_{1.5}Ge_1$ alloys heat treated at various temperatures. Estimated errors in B_{hf} were ±0.5 T, in I was ±1%, and in IS were ±0.01 mm/s.

Samples			As-spun	400 °C	480 °C	560 °C	640 °C	730 °C
Al_0Ge_0	A_1	B_{hf} (T)	23.4	24.1	20.9	16.8	0.0	0.0
		I (%)	30	28	12	42	13	9
		δ (mm/s)	0.23	0.24	0.27	0.11	0.05	0.03
	A_2	B_{hf} (T)	21.5	22.0	20.1			
		I (%)	55	56	53			
		δ (mm/s)	0.06	0.05	0.06			
	A_3	B_{hf} (T)	12.8	13.5	10.8			
		I (%)	15	17	5			
		δ (mm/s)	0.01	0.02	0.02			
	A_4	B_{hf} (T)			19.2	19.5	19.3	19.3
		I (%)			3	12	14	15
		δ (mm/s)			0.25	0.26	0.25	0.24
	A_{5a}	B_{hf} (T)			24.6	24.4	24.0	24.0
		I (%)			21	14	20	23
		δ (mm/s)			0.20	0.19	0.23	0.23
	A_{5b}	B_{hf} (T)					23.6	23.6
		I (%)					15	13
		δ (mm/s)					0.05	0.05
	A_6	B_{hf} (T)				28.5	28.5	28.5
		I (%)				12	14	14
		δ (mm/s)				0.09	0.10	0.11
	A_7	B_{hf} (T)			30.8	31.1	31.1	31.3
		I (%)			6	11	12	12
		δ (mm/s)			0.07	0.08	0.07	0.07
	A_8	B_{hf} (T)				32.5	32.4	32.5
		I (%)				9	12	13
		δ (mm/s)				0.05	0.05	0.06
		Crstal. %			31	58	87	91
		θ (deg)	65	71	71	71	57	57
$Al_{1.5}Ge_1$	A_1	B_{hf} (T)	22.5	23.5	18.9	14.5	0.0	0.0
		I (%)	26	26	61	36	14	9
		δ (mm/s)	0.26	0.26	0.11	0.15	0.08	0.07
	A_2	B_{hf} (T)	21	21.5				
		I (%)	61	58				
		δ (mm/s)	0.07	0.07				
	A_3	B_{hf} (T)	11.6	12.6				
		I (%)	13	16				
		δ (mm/s)	0.01	0.01				
	A_4	B_{hf} (T)			19.9	19.8	19.7	19.7
		I (%)			17	23	24	28

TABLE I. (*Continued.*)

Samples			As-spun	400 °C	480 °C	560 °C	640 °C	730 °C
		δ (mm/s)			0.26	0.26	0.26	0.25
	A_{5a}	B_{hf} (T)			24.6	24.6	24.2	24.4
		I (%)			11	14	18	19
		δ (mm/s)			0.22	0.18	0.24	0.25
	A_{5b}	B_{hf} (T)					23.8	23.9
		I (%)					16	14
		δ (mm/s)					0.05	0.06
	A_6	B_{hf} (T)			29.3	28.2	28.6	28.7
		I (%)			3	7	9	9
		δ (mm/s)			0.17	0.09	0.12	0.12
	A_7	B_{hf} (T)			31.1	30.8	31.0	31.4
		I (%)			9	13	12	11
		δ (mm/s)			0.08	0.08	0.08	0.08
	A_8	B_{hf} (T)				32.0	32.2	32.3
		I (%)				7	7	9
		δ (mm/s)				0.06	0.05	0.05
		Crstal. %			39	64	85	91
		θ (deg)	59	68	68	68	57	57

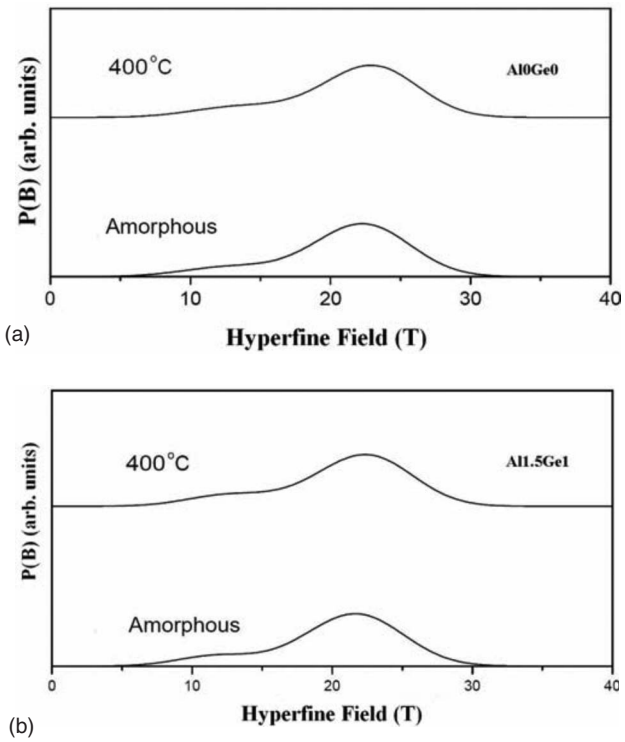

FIG. 12. Magnetic hyperfine field distributions $P(B_{hf})$ for both series of as-spun and heat-treated alloys at 400 °C: (a) Al_0Ge_0 and (b) $Al_{1.5}Ge_1$.

zian lines corresponding to different Fe neighborhoods in the Fe-Si phase and a Gaussian line shaped distribution for the amorphous phase. The components with magnetic hyperfine fields (B_{hf}) about 19.5, 24.5, 28.5, 31.0, and 32 T could be assigned to four (A_4), five (A_5), six (A_6), seven (A_7), and eight (A_8 and D) iron near-neighbor sites, respectively, attributed to the $D0_3$ Fe(Si) phase, in agreement with Ref. 31 (Table I). The analysis of the Mössbauer spectra for both series of alloys annealed at 560 °C revealed the presence of two phases, a residual amorphous phase with a reduced hyperfine field (16.9 T) compared to those of amorphous alloys, i.e., ~22.5 T for $Al_{1.5}Ge_1$ and ~23.4 T for Al_0Ge_0 alloys, and the Fe_3Si phase with $D0_3$ structure (Table I). Annealing of an amorphous alloy normally leads to an enhanced hyperfine field due to an increase in density. Here, the

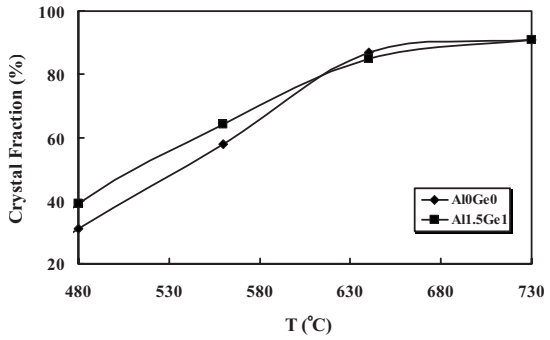

FIG. 13. Variations of crystalline fraction (in %) versus heat-treatment temperatures for both series of alloys studied.

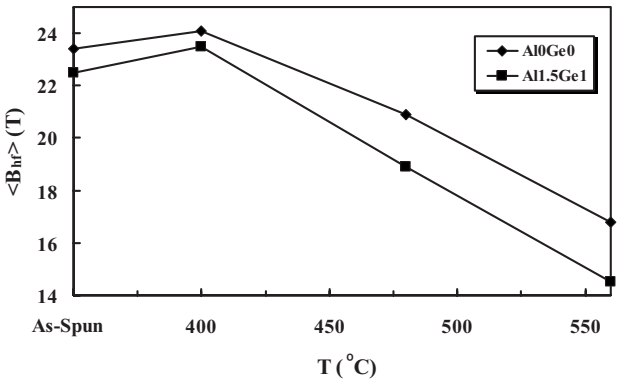

FIG. 14. Variations of the average $\langle B_{\mathrm{hf,am}} \rangle$ versus heat-treatment temperature.

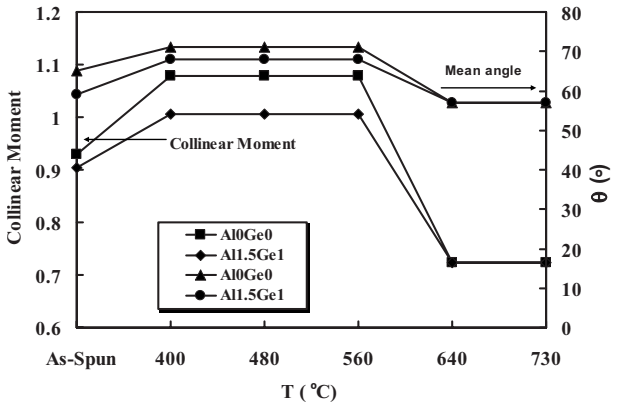

FIG. 15. Variations of mean magnetic moment ($\bar{\theta}$) as well as collinear magnetic moment versus heat-treatment temperatures for both series of alloys studied.

amorphous phase is depleted in iron, thus exhibiting a decreased hyperfine field. Further, as Table I demonstrates, the magnitudes of the hyperfine field (B_{hf}) and the IS of the A_6 site for the $Al_{1.5}Ge_1$ alloy heat treated at 480 °C were 29.3 T and 0.17 mm/s, respectively. These were 28.2 T and 0.09 mm/s for this alloy when heat treated at 560 °C. The reduction of the B_{hf} and IS for the latter highlights the possible substitution of Al atoms with large atomic radius for Fe atoms. IS can be affected by atomic size, electronegativity, or number of outer electrons. Furthermore, for both series of alloys heat treated at 640 and 730 °C, an additional Zeeman sextet of two components around 24 T with different IS (Table I) is observed, which is attributed to the formation of the Fe-B phase, in agreement with our XRD, DSC, and TEM results.

Mössbauer spectroscopy can also be used to determine the distribution of magnetic moment directions in magnetic materials. The mean angle $\bar{\theta}$ between the magnetic moments and the direction of incident γ ray is determined by[32]

$$\bar{\theta} = \sin^{-1}\left[\frac{6(A_{2,5}/A_{1,6})}{4+3(A_{2,5}/A_{1,6})}\right]^{1/2}, \tag{1}$$

where $A_{1,6}$ and $A_{2,5}$ are the areas of peaks 1 and 6, and 2 and 5, respectively. The ratio of

$$\frac{A_{2,5}}{A_{1,6}} = \frac{4\sin^2\bar{\theta}}{3(1+\cos^2\bar{\theta})} \tag{2}$$

is defined as the collinear moment. Hence, the collinear moments are dependent on the magnetic orientation. When the incident γ ray is parallel to the magnetic moment orientation, the angle will be zero and the collinear moments will be also zero. However, when the incident γ ray is perpendicular to the magnetic moment orientation, the angle will be 90°, and then the collinear moments will be 1.33. For a random orientation of magnetic moments, the collinear moments will be averaged with respect to different angles and result in a value of 0.67.[33] The variations of collinear magnetic moment and $\bar{\theta}$ against heat-treatment temperatures is shown in Fig. 15, based on refined Mössbauer data. It should be mentioned that in our experiment, the incident γ ray was perpendicular to the ribbon axis.

As can be realized from Fig. 15, for both series of as-spun alloys, the collinear moments and the moment mean angle ($\bar{\theta}$) were low due to the stresses introduced during the melt spinning process.[33] However, their magnitudes increased when heat treated above 400 °C due to the stress relief and the formation of the exchange coupled Fe_3Si phase at higher temperature. In such a case, the resulting magnetoelastic anisotropy will be very small due to the compensation of the negative magnetostriction of the Fe-Si phase by the positive magnetostriction of the amorphous matrix.[34] The lower collinear magnetic moment angles observed for the as-spun samples (Fig. 15) suggest that the magnetic moments were not completely parallel to the ribbon axis direction. For the samples heat treated at 640 and 730 °C, again, a sharp decline in the magnitudes of $\bar{\theta}$ and collinear moments appeared (Fig. 15), which is due to the presence of the hard magnetic boride phase that developed along with the Fe_3Si phase for both series of alloys.

C. Magnetic properties

Figure 16 displays the variation of saturation induction (B_S) as well as coercivity ($_BH_C$) versus heat-treatment temperature. As can be realized from this graph, a rising trend was observed for B_S values with increasing the temperature and the highest values of B_S were obtained for both series of alloys heat treated at 560 °C. The observed rise of the B_S for the samples heat treated up to 480 °C is mainly related to stress relief that happened due to the relaxation processes taking place and the onset of partial crystallization of Fe-Si phase. The higher B_S values obtained for both series of alloys heat treated at 560 °C (Fig. 16) is due to the higher level of formation of the nanocrystalline Fe_3Si phase, as confirmed by our XRD and Mössbauer results (Fig. 13). However, the magnitudes of B_S were lower for all of the heat-treated $Al_{1.5}Ge_1$ samples compared to those of Al_0Ge_0 alloys (Fig. 16), despite the rather higher degree of crystallization observed for the $Al_{1.5}Ge_1$ alloys (Fig. 13).

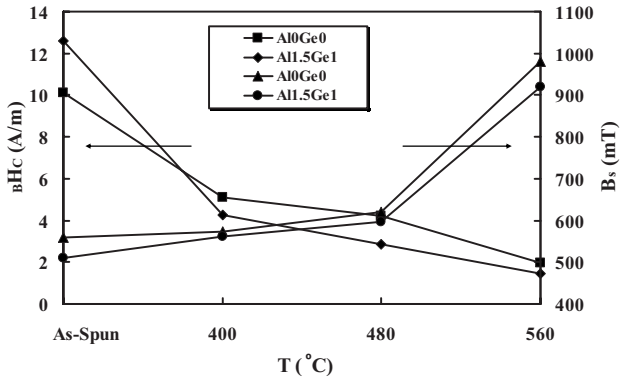

FIG. 16. Variations of saturation induction (B_S) and coercive field ($_BH_C$) versus heat-treatment temperatures for both series of alloys studied.

It should be mentioned that, for a magnetic nanocomposite system, one should realize that the saturation magnetization (M_S), and hence B_S, depends on the crystalline volume fraction (x) through the proportion of the different phases contributing to the total magnetization of the sample by considering that

$$M_S = M_{\mathrm{am}}(1-x) + M_{\mathrm{cr}}(x), \tag{3}$$

where M_{am} and M_{cr} are the saturation magnetization for the amorphous and crystalline phases, respectively. The observed lower values of B_S for the $Al_{1.5}Ge_1$ alloys heat treated between 400 and 560 °C compared to those of Al_0Ge_0 alloys are mainly due to the comparatively lower Fe concentration used for the former and substitution of nonmagnetic elements such as Al or Ge for Fe atoms in the Fe_3Si lattice. The variations of $_BH_C$ versus heat-treatment temperatures for both series of alloys (Fig. 16) can be divided into two distinct regions: the first one is a sharp declining trend appearing between as-spun samples and those heat treated at 400 °C for which no signs of formation of nanocrystalline Fe_3Si phase could be detected (Figs. 1 and 2) and the second region is that observed for the samples heat treated between 400 and 560 °C. Further, the magnitudes of the $_BH_C$ for both series of alloys heat treated at 640 and 730 °C were drastically increased and reached ~6400 A/m, which is well above that of a soft magnetic material.

The observed sharp decline of $_BH_C$ values for the two series of as-spun alloys during the initial stage of heat treatment at 400 °C (Fig. 16) is mainly related to the decrease of magnetostriction.[35] Magnetostriction anisotropy is governed by the alloy composition, which determines the magnetostriction constant (λ) and stress field which results from the fabrication process. It is interesting to mention that the magnitude of the $_BH_C$ value was higher in the case of the as-spun $Al_{1.5}Ge_1$ sample compared to that of the Al_0Ge_0 alloy. This is possibly related to the existence of a higher level of remaining stresses due to the presence of Al atoms of larger atomic radius size compared to that of Fe atoms. However, the setup of the excellent soft magnetic properties for the samples heat treated at 560 °C (Fig. 16) is related to the sharp decline of both the magnetocrystalline and magnetostrictive anisotropies. For appropriately heat-treated FINEMET alloys, the positive magnetostriction of the residual amorphous phase ($\lambda_{\mathrm{sam}}=20\times10^{-6}$) is balanced with the negative magnetostriction of the growing Fe(Si) nanocrystalline phase ($\lambda_{\mathrm{FeSi}}=-6\times10^{-6}$).[34,36] The origin of the excellent soft magnetic properties observed for the samples heat treated at 560 °C lies in the nanometric grain sizes of the Fe_3Si phase which is lower than the exchange-correlation length.[37]

Based on the random anisotropy model developed by Herzer,[37] it is known that the effective anisotropy contribution of the small randomly oriented bcc Fe(Si) grains is essentially reduced by exchange interaction. The critical scale where the exchange energy states balance the anisotropy energy is $L_0=(A/K_1)^{1/2}$, where L_0 is the exchange-correlation length, A is the exchange stiffness constant, and K_1 is the magnetocrystalline anisotropy. L_0 takes the value of about 35 nm for bcc Fe-Si (20 at. %), which determines the order of the domain wall width. For $D\approx L_0/3$, i.e., grain sizes of the order of 10–15 nm, the magnetization will not follow the randomly oriented easy axis of the individual grains, but increasingly is forced to align parallel by exchange interaction. As a consequence, the local anisotropies are averaged out over an increasing number of grains such that the effective anisotropy constant K_{eff} finally scales down as[37,38]

$$K_{eff} \sim KD^{3/2} \sim \left(\frac{K_{eff}}{A}\right)^{3/2} \sim \left(\frac{K^4D^6}{A^3}\right), \tag{4}$$

where K is the magnetocrystalline anisotropy constant of any grain and the D is the average grain size. Since the coercivity (H_C) can be considered as proportional to the effective anisotropy,[37] one can predict a similar variation of H_C with average grain size. The observed decrease of the $_BH_C$ for both series of alloys heat treated at 560 °C can be taken as partly due to the decrease of the effective magnetocrystalline anisotropy constant and partly due to the sharp decline of the magnetostriction. As mentioned before, based on the Herzer model[37] for nanocrystalline soft magnetic material, the exchange between the anisotropic grains takes place through the amorphous matrix. Considering that the exchange-correlation length of the amorphous matrix is generally longer than the intergranular average distance, the grains can be considered coupled and behave similarly to a single phase system. However, the role of residual amorphous matrix is much more pronounced in the initial stage of nanocrystallization[39,40] and close to the paramagnetic transition of the amorphous matrix.[41] In fact, for a microstructure with low crystallization fraction (x) or finite values of exchange-correlation length of the amorphous matrix, Herzer's model does not fit properly. This model was later modified[41] to account for the two phase character of the microstructure in terms of the volume fraction of the crystallites. Based on the model developed by Hernando *et al.*,[41] it is shown that the coercivity for either magnetization rotation or wall motion can be expressed by

$$H_C = P_C\left(\frac{\langle K\rangle + K_{\mathrm{am}}}{\mu_0 M_S}\right)\left(1-\sqrt{\frac{25k_BT}{\langle K\rangle V}}\right) \tag{5}$$

where P_C is a dimensionless factor close to unity, V is the volume of single domain grains, K_{am} is the anisotropy con-

stant of the amorphous matrix, $\langle K \rangle$ is the average structural anisotropy of the nanocrystalline phase, M_S is the sample saturation magnetization, and k_B is Planck's constant. In Eq. (5), the second term represents the absence of coercivity in the superparamagnetic regime, which becomes dominated in the case of fully decoupled crystallites having sufficiently large interparticle distances. It is already shown that for the samples of a large number of densities of particles, the interactions between the grains result in ordering of magnetic moments and prevent superparamagnetic relaxation.[42,43] For such a case and for the condition that grain size (D) is smaller than the structural correlation length and for mutually fully coupled nanocrystals, the coercivity is shown to be[41]

$$H_C = P_C \frac{x^2 K_1^4 D^6}{\mu_0 M_S A_{\text{eff}}^3} + P_C \frac{K_{\text{am}}}{\mu_0 M_S} \tag{6}$$

where x is the volume fraction of the nanocrystalline phase, K is the magnetocrystalline anisotropy of the crystallites, D is the grain size, and A_{eff} is the effective exchange constant which is determined by the exchange constant of the amorphous matrix rather than that of the Fe-Si crystallites. Equation (6) expresses the magnetic hardening normally observed for low crystalline volume fraction[44] and for the condition near the ferromagnetic-paramagnetic transition of the amorphous phase.[37] For both series of alloys heat treated below 480 °C whose low x values were detected, the existence of a rather high concentration of superparamagnetic phases can be expected. Therefore, the overall coercivity of such a microstructure could be partly influenced by the existence of the superparamagnetic phase. However, by increasing the heat-treatment temperature to 560 °C, the average grain sizes of both series of alloys increase (Fig. 6) and hence the superparamagnetic contribution diminishes by the growing sizes of Fe_3Si crystallites and the magnitude of the overall coercivity will mainly follow Eq. (6). For the samples heat treated between 400 and 560 °C, as our Mössbauer results revealed, the magnitude of x increases (Fig. 13), and hence the first term of Eq. (6) will mainly express the coercivity of these alloys.

Unfortunately, the model of Hernando *et al.*[41] has one major shortcoming related to the presence of magnetostriction anisotropy in the early stage of crystallization where the effects of stress anisotropy cannot be ignored. Magnetostriction is another important magnetic property of a magnetic material which gives rise to the magnetoelastic anisotropy, although due to the complex status of the internal stresses and strains, magnetoelastic interactions, and the density of topological defects arising from interfaces of different phases, the interpretation of the magnetostriction is not an easy task. It is shown that the effective magnetostriction (λ_{eff}) consists of three contributing sources related to the Fe-Si crystalline phase, amorphous matrix, and crystalline-amorphous interface.[38] This is shown to be expressed by[45]

$$\lambda_{\text{eff}} = x\lambda_{\text{cr}} + (1-x)(\lambda_{\text{am}} + kx) + 3x\lambda_{\text{surf}}/R, \tag{7}$$

where λ_{cr} is the crystalline magnetostriction constant of the Fe-Si phase which depends on Si concentration, λ_{am} is the amorphous matrix magnetostriction constant, k is a parameter describing the evolution of the amorphous matrix magnetostriction, R is the average radius of Fe-Si crystallites, and x is the fraction of crystallinity. It is also already shown that λ_{eff} decreases sharply with the increase of crystalline fraction and the rise of grain size.[45] Therefore, in the early stage of crystallization, a higher value of λ_{eff} is expected due to a lower x value and a higher coercivity can be expected,[46] as also seen in the cases of both series of Al_0Ge_0 and $Al_{1.5}Ge_1$ alloys in the as-spun state and when heat treated at temperatures below 560 °C (Fig. 16). However, for the optimum microstructure developed for both series of alloys when heat treated at 560 °C, the two main contributing sources of magnetostriction, i.e., λ_{cr} and λ_{am}, counterbalance each other and the overall λ_{eff} reduces drastically. Considering the above mentioned issues, the total coercivity in nanocrystalline alloys such as FINEMET will have contributing terms originated from intrinsic fluctuations of exchange energies and/or local anisotropy, magnetoelastic coupling, and that of clusters and/or nanocrystals.

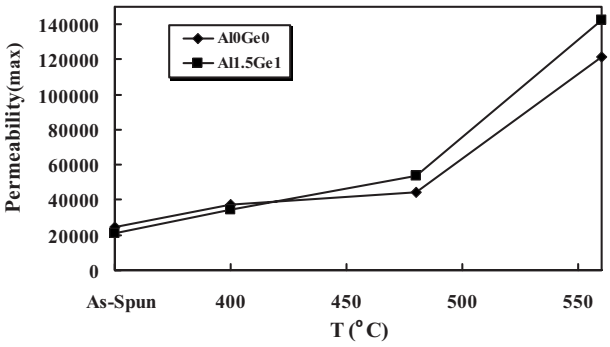

FIG. 17. Variations of maximum magnetic permeability (μ_S) versus heat-treatment temperatures for both series of alloys studied.

Further, It is interesting to note that the magnitudes of ${}_BH_C$ for the $Al_{1.5}Ge_1$ alloys heat treated at 400, 480, and 560 °C were lower compared to those of pure FINEMET samples (Fig. 16). This is believed to be related to the decline of the magnetocrystalline anisotropy in $Al_{1.5}Ge_1$ alloy. The formation of the boride phase confirmed by our XRD and TEM measurements for both series of alloys heat treated at 640 and 730 °C deteriorated the observed excellent soft magnetic properties (Fig. 16). This was due to both the sharp rise of the average grain sizes of these samples [Fig. 9(a)] well above the exchange-correlation length, as confirmed by our TEM results, and the larger magnetocrystalline anisotropy constant of the Fe_2B phase compared to that of the Fe_3Si phase.[47] The setup of the ultrasoft magnetic properties for both series of alloys heat treated at 560 °C was also confirmed by maximum magnetic permeability (μ_{max}) measurements. Figure 17 demonstrates the variation of μ_{max} versus the heat-treatment temperature.

Here, the observed rising trend of μ_{max} with rising heat-treatment temperature (Fig. 17) is also in close agreement with the trend observed for B_S and ${}_iH_C$. In general, $Al_{1.5}Ge_1$ alloy heat treated at 560 °C showed superior soft magnetic properties compared to Al_0Ge_0 alloy. Furthermore, the magnitudes of the Curie temperatures of the ferromagnetic amor-

phous phase ($T_{C,\mathrm{am}}$) for Al_0Ge_0 and $Al_{1.5}Ge_1$ alloys obtained from their corresponding DSC graphs were 317 and 322 °C, respectively. The observed rise of $T_{C,\mathrm{am}}$ for the $Al_{1.5}Ge_1$ alloy was in agreement with previous report on Ge added FINEMET alloy.[14] The Curie temperature of the amorphous phase ($T_{C,\mathrm{am}}$) is sensitive to changes in short range order. Further, T_C depends on the average distance between magnetic atoms, and its increase could be possibly associated to a decrease in Fe-Fe distance. However, the substitution of Al in small quantities (up to 3 at. %) for Fe atoms in FINEMET alloys has already been reported[10] to decrease the Curie temperature of Fe-Si crystallites and increase that of the amorphous matrix compared to the pure FINEMET alloy. Replacing Fe with Al atoms in the Fe-Si phase changes the local environment of some of the Fe atoms and can give rise to the exchange weakening of two neighboring Fe atoms. This can give rise to a lower T_C for the Fe-Si phase and the reduction of magnetic moment as well. Based on our Mössbauer results and previous 3DAP analysis carried out on 2 at. % Al added FINEMET alloy,[10] which confirmed the presence of Al in the Fe_3Si phase rather than the amorphous matrix, we assume that the rise of $T_{C,\mathrm{am}}$ for $Al_{1.5}Ge_1$ compared to that of Al_0Ge_0 could be mainly related to Ge atom. However, this demands further study by other techniques such as 3DAP (arranged to be done).

IV. CONCLUSIONS

The coaddition of Al/Ge in small quantities was found to increase the maximum magnetic permeability and ferromagnetic amorphous phase Curie temperature ($T_{C,\mathrm{am}}$) and reduce coercivity compared to those of pure FINEMET alloy when heat treated at 560 °C for 1 h. The decrease of the latter is related to the decrease of magnetocrystalline anisotropy due to the substitution of Al for Fe atoms, as evidenced by our Mössbauer and XRD results. The increase in $T_{C,\mathrm{am}}$ is also possibly related to the presence of Ge in the amorphous phase. However, this demands further study. The formation of Fe_3Si phase of $D0_3$ structure was confirmed for all of the samples heat treated at 560 °C for 1 h in an amorphous matrix based on our XRD, TEM, and Mössbauer results. Further, for all of the samples heat treated above 560 °C, the formation of the Fe-Nb-B second phase was detected. The formation of this phase and the increased grain sizes observed for these alloys deteriorated the excellent soft magnetic properties for both series of alloys heat treated above 560 °C.

ACKNOWLEDGMENTS

We would like to acknowledge the help of the Advanced Material Research Center at the Department of Metallurgy and Materials Engineering of the Iran University of Science and Technology (IUST) and the Ministry of Industries and Mines for support (F.S.) We also acknowledge the help of S. Kamali from the Department of Physics, Angstrom Laboratory, Uppsala University, Sweden, for his kind help with Mössbauer analysis. Finally, R. Schierholz from the Technical University of Darmstadt and N. Wanderka from the Hahn-Meitner-Institut Berlin GmbH are also acknowledged for their kind collaboration regarding the TEM investigations.

*Corresponding author: beitolla@iust.ac.ir

[1] M. E. McHenry, M. A. Willard, and D. E. Laughlin, Prog. Mater. Sci. **44**, 291 (1999).
[2] P. Gorria, V. M. Prida, M. Tejedor, B. Hernando, and H. L. Sanchez, Physica B **299**, 215 (2001).
[3] V. M. Prida, P. Gorria, G. V. Kurlyandskaya, M. L. Sanchez, B. Hernando, and M. Tejedor, Nanotechnology **14**, 231 (2003).
[4] M.-H. Phan, H.-X. Peng, M. R. Wisnom, and S.-C. Yu, J. Appl. Phys. **98**, 014316 (2005).
[5] M. E. McHenry and D. E. Laughlin, Acta Mater. **48**, 223 (2000).
[6] J. Gonzalez, N. Murillo, J. M. Blanco, J. M. Gonzalez, and T. Kulik, J. Appl. Phys. **76**, 1131 (1994).
[7] V. Franco, C. F. Conde, A. Conde, and P. Ochin, J. Non-Cryst. Solids **287**, 366 (2001).
[8] J. M. Borrego, C. F. Conde, and A. Conde, Mater. Sci. Eng., A **304-306**, 491 (2001).
[9] M. Frost, I. Todd, H. A. Davies, M. R. J. Gibbs, and R. V. Major, J. Magn. Magn. Mater. **203**, 85 (1999).
[10] T. Szumiata, B. Gorka, A. Zorkovska, and P. Sovak, J. Magn. Magn. Mater. **295**, 95 (2005).
[11] E. Illekova, P. Duhaj, and M. Jergel, J. Non-Cryst. Solids **287**, 167 (2001).
[12] L. K. Varga, F. Mazaleyrat, Gy. Kovacs, and A. Kakay, J. Magn. Magn. Mater. **226-230**, 1550 (2001).
[13] J. S. Blazquez, V. Franco, C. F. Conde, and A. Conde, J. Magn. Magn. Mater. **254-255**, 460 (2003).
[14] V. Cremaschi, G. Sanchez, and H. Sirkin, Physica B **354**, 213 (2004).
[15] B. D. Cullity, in *Elements of X-Ray Diffraction* (Addison Wesley, Reading, MA, 1987), p. 284.
[16] G. K. Williamson and W. H. Hall, Acta Metall. **1**, 22 (1953).
[17] K. Lagarec and D. C. Rancourt, RECOIL, Mössbauer spectral analysis software for Windows, Version 1.0, 1998.
[18] The International Union of X-ray Crystallography Structure Report No. 9, 1942 (unpublished).
[19] W. B. Pearson, *Handbook of Lattice Spacings and Structure of Metals and Alloys* (Pergamon, Oxford, 1964).
[20] P. J. Warren, I. Todd, H. A. Davies, A. Cerezo, M. R. J. Gibbs, D. Kendall, and R. V. Major, Scr. Mater. **41**, 1223 (1999).
[21] K. Hono, K. Hiraga, Q. Wang, A. Inoue, and T. Sakurai, Acta Metall. Mater. **40**, 2137 (1992).
[22] I. Matko, P. Duhaj, P. Svec, and D. Janickovic, Mater. Sci. Eng., A **179-180**, 557 (1994).
[23] M. H. Phan, H.-X. Peng, M. R. Wisnom, S.-C. Yu, and N. Chau, Composites, Part A **37**, 191 (2006).
[24] I. Z. Rahman, M. d. Kamruzzaman, and M. A. Rahman, Phys. Status Solidi C **1**, 3632 (2004).
[25] J. M. Borrego, A. Conde, V. A. Pena-Rodriguez, and J. M.

Greneche, Hyperfine Interact. **131**, 67 (2000).
[26] R. Juhasz, A. Cziraki, L. F. Kiss, and A. Lovas, Mater. Sci. Eng., A **375-377**, 1057 (2004).
[27] M. Ohnuma, K. Hono, S. Linderoth, J. S. Pedersen, Y. Yoshizawa, and H. Onodera, Acta Mater. **48**, 4783 (2000).
[28] M. Miglierini, J. Phys.: Condens. Matter **6**, 1431 (1994).
[29] P. P. Marci, P. Rose, D. E. Bonda, N. Cowlam, G. Principi, and S. Enzo, Mater. Sci. Forum **179-181**, 249 (1995).
[30] K. Hono, D. H. Ping, M. Ohnuma, and H. Onodera, Acta Mater. **47**, 997 (1999).
[31] M. B. Stearns, Phys. Rev. **129**, 1136 (1963).
[32] A. G. Maddock, *Mössbauer Spectroscopy, Principles and Applications* (Horwood, Chichester, 1997).
[33] X. D. Li, W. Z. Yuan, Z. J. Zhao, X. Z., Wang, J. Z. Ruan, and X. L. Yang, J. Magn. Magn. Mater. **279**, 429 (2004).
[34] G. Herzer, in *Encyclopedia of Materials: Science and Technology*, edited by K. H. V. Buschow (Elsevier, Amsterdam, 2001), p. 5897.
[35] G. Vlasak, Z. Kaczkowski, P. Svec, and P. Duhaj, Mater. Sci. Eng., A **226-228**, 749 (1997).
[36] M. Tejedor, B. Hernando, M. L. Sanchez, V. M. Prida, J. M. Gracia-Beneytez, M. Vazquez, and G. Herzer, J. Magn. Magn. Mater. **185**, 61 (1998).
[37] G. Herzer, IEEE Trans. Magn. **25**, 3327 (1989).
[38] G. Herzer, Mater. Sci. Eng., A **133**, 1 (1991).
[39] M. Vazquez, P. Marin, A. O. Olofinajana, and H. A. Davies, Appl. Phys. Lett. **64**, 3184 (1994).
[40] C. Gomez-Polo, D. Holzer, M. Multigner, E. Navarro, P. Agudo, A. Hernando, M. Vazquez, H. Hassik, and R. Grossinger, Phys. Rev. B **53**, 3392 (1996).
[41] A. Hernando, P. Marin, M. Vazquez, J. M. Barandiaran, and G. Herzer, Phys. Rev. B **58**, 366 (1998).
[42] A. Hernando and T. Kulik, Phys. Rev. B **49**, 7064 (1994).
[43] P. Marin, M. Vazquez, and A. Hernando, J. Magn. Magn. Mater. **196-197**, 221 (1998).
[44] Y. Yoshizawa, S. Oguma, and K. Yamauchi, J. Appl. Phys. **64**, 6044 (1998).
[45] T. Szumiata, K. Brzozka, M. Gawronski, B. Gorka, J. S. Blazquez-Gamez, T. Kulik, R. Zuberek, and A. Slawska-Waniewska, J. Magn. Magn. Mater. **272-276**, 1443 (2004).
[46] J. S. Blazquez, V. Franco, and A. Conde, J. Phys.: Condens. Matter **14**, 11717 (2002).
[47] G. Herzer, J. Magn. Magn. Mater. **294**, 99 (2005).